Constraining the age of the last geomagnetic reversal from geochemical and magnetic analyses of Atlantic, Indian, and Pacific Ocean sediments

Jean-Pierre Valet, Franck Bassinot, Quentin Simon, Tatiana Savranskaia, Nicolas Thouveny, Didier Bourlès, Anouk Villedieu

Earth and Planetary Science Letters 506 (2019) 323–331

Contents lists available at ScienceDirect

Earth and Planetary Science Letters

www.elsevier.com/locate/epsl

Constraining the age of the last geomagnetic reversal from geochemical and magnetic analyses of Atlantic, Indian, and Pacific Ocean sediments

Jean-Pierre Valet [a], Franck Bassinot [b,*], Quentin Simon [c], Tatiana Savranskaia [a], Nicolas Thouveny [c], Didier L. Bourlés [c], Anouk Villedieu [b]

[a] Institut de Physique du Globe de Paris, Université Paris Diderot, Sorbonne Paris-Cité, UMR 7154 CNRS, 1 rue Jussieu, 75238 Paris Cedex 05, France
[b] Laboratoire des Sciences du Climat et de l'Environnement (CEA-CNRS-UVSQ), Domaine du CNRS, Avenue de la Terrasse, 91198 Gif-sur-Yvette, France
[c] CEREGE UM34, Aix Marseille Univ., CNRS, IRD, INRA, Coll France, Aix-en-Provence, France

ARTICLE INFO

Article history:
Received 9 February 2018
Received in revised form 2 September 2018
Accepted 4 November 2018
Available online 20 November 2018
Editor: B. Buffett

Keywords:
magnetic reversal
Brunhes–Matuyama
Be-ratio
field intensity
stratigraphy

ABSTRACT

We studied four marine sediment records of the Matuyama–Brunhes geomagnetic reversal from four sites located in the Indian, Atlantic and western Pacific oceans. The results combine paleomagnetic, cosmogenic nuclide beryllium (^{10}Be) and oxygen isotope analyses that were performed on the same samples in order to avoid any stratigraphic bias. The three records from the equatorial Indian Ocean and North Atlantic Ocean did not reveal any offset between the authigenic ^{10}Be/^{9}Be ratio (Be-ratio) peak and the interval of low relative paleointensity (RPI) that characterizes the reversal. The lower and upper limits of transitional directions are also concomitant with the increased atmospheric ^{10}Be production that accompanied the geomagnetic dipole intensity decrease. In contrast, the record from western equatorial Pacific Ocean sediments was found 18 cm below the Be-ratio changes as a result of late magnetization acquisition. At all four sites, maximum ^{10}Be production occurred at the same period soon after the maximum of Marine Isotope Stage 19 (MIS 19) and, therefore, indicates its synchronous worldwide character. Such features are effectively observed from the Be-ratio signals and their relationship with the magnetic transition interval, which further confirms the synchronous character of the transition. Taking all dating uncertainties (1.6 ka between sites and 5 ka for the age model) into consideration, our records suggest a mean reversal age of 772.4 ± 6.6 ka. The age of the transition in the Atlantic Ocean record is closer to 774 ka but this difference is within the limit of significance.

1. Introduction

The age of the last reversal is constrained by orbitally tuned oxygen isotope records of marine sediments and by radiometric ages that have been mostly obtained from volcanic material. In the first case, there is a large consensus for a 773 ka transition, whereas some recent controversial radiometric datings of tephra layers (Singer and Pringle, 1996; Singer et al., 2002; Mark et al., 2017) conclude in favor of a 10 kyr older age. A dating range of nearly 12 kyr exists for the last reversal between studies that presents younger ages commonly averaged at 773 ka (e.g. Channell et al., 2010; Valet et al., 2014) and older ages centered at 785 ka (e.g. Sagnotti et al., 2016; Mark et al., 2017). Such differences may seem relatively insignificant and without consequence for our knowledge of the geodynamo or for the mechanisms for reversals. However, the accuracy of age determinations constrains our ability to reconstruct properly the phase relationship among records (e.g. geomagnetic and climatic) from different locations. Precision on reversal ages may also affect various studies such as statistical analyses of the geomagnetic polarity time scale or research on possible links between Earth's orbital parameters and geomagnetic changes (Worm, 1997; Courtillot et al., 2007; Thouveny et al., 2008).

Two important aspects must be considered before attempting to provide an accurate age estimate for the last reversal. The first concerns the synchronism of polarity changes at different locations, especially at different latitudes. By definition, any evolution of the dipole field, specifically its pre-transitional decay and subsequent growth in the opposite polarity, occurs synchronously all over the Earth and can, thus, be described by records of relative paleointensity (RPI) and/or by production of cosmogenic isotopes. This is not the case when referring to transitional directions between the two polarities that emerge when the dipole field intensity drops to a threshold limit (about 20% of the present geomagnetic intensity (see e.g., Valet and Plenier, 2008; Balbas et al., 2018). There is an overall consensus that transitional directions are associated

* Corresponding author.
E-mail address: Bassinot@lsce.ipsl.fr (F. Bassinot).

https://doi.org/10.1016/j.epsl.2018.11.012

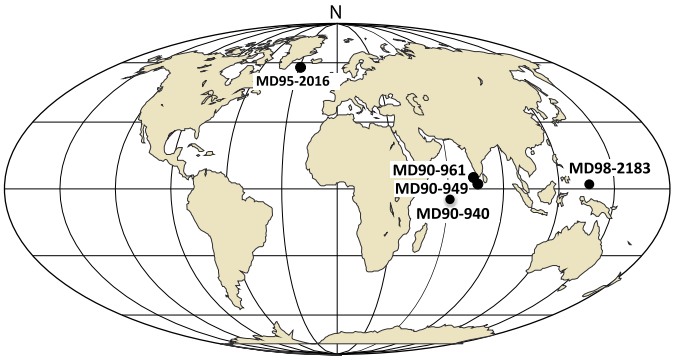

Fig. 1. Location map of the core sites. Red labels indicate the four sites primarily involved in this study. Also shown is the position of core MD90-940 that was used for the microtektite study. (For interpretation of the colors in the figure(s), the reader is referred to the web version of this article.)

with a multipolar field geometry (see Valet and Fournier, 2016; Balbas et al., 2018). Such phases might, therefore, not be perfectly synchronous at the Earth's surface. Scarcity of transitional directions in volcanic reversal records and estimates derived from high-resolution sedimentary records indicate that the transitional period does not exceed a few thousand years (Channell, 2017; Valet et al., 2012), with controversial estimates (Evans and Muxworthy, 2018) of only a few years (Sagnotti et al., 2016), and represents only 10 to 20% of the full reversal process in contrast to field intensity changes.

A Bayesian inversion model of the last reversal suggests that the onset of the transition may have not been synchronous around the Earth (Leonhardt and Fabian, 2007). However, despite the pertinence of the method, the conclusions of the analysis are controversial because several records on which the simulation is based are demonstrably wrong (see Valet and Fournier, 2016; Channell, 2017). Numerical simulations have also shown a possible time lag between records that basically depends on the location within the Earth's liquid core where reversed flux starts to propagate (Olson et al., 2011). Recently, Kong et al. (2014) mentioned a discrepancy between the reversal positions in Chinese loess–paleosol sequences (Zhao and Roberts, 2010; Wang et Lovlie, 2010) and marine sediment cores, but several studies (Wang et al., 2014; Zhou et al., 2014) emphasize that post-depositional remagnetizations rule out the pertinence of loess sequences for studying magnetization variations over such short time periods.

Contrasting transitional behavior caused by complex field morphology leads us to the second aspect that concerns the definition of transition boundaries and the choice of the parameter used to describe geomagnetic changes. As discussed above, the reversal process is constrained by locally varying non-dipolar fields while dipolar variations must be seen as universal. Therefore, the reversal age can change if we refer to the onset of the field decline compared to the onset of directional changes, or to any indicator used to define the mid-point of the transition.

Based on these considerations we selected four sediment cores (Fig. 1) that recorded the last reversal from the Atlantic, Indian and Pacific oceans (Fig. 1). Magnetic records have been published for some of these cores (Valet et al., 2014, 2016), but they have been revisited in order to reduce stratigraphic uncertainty. A major characteristic of the present study is that we rely on magnetic, authigenic $^{10}Be/^{9}Be$ ratio (Be-ratio hereafter), and oxygen isotope data that were obtained from samples from the exact same depths in the four sedimentary records to investigate the phase relationship among the parameters and, therefore, to determine precisely the limits of the reversal phase. We also identified the Australasian microtektite layer that defines an instantaneous stratigraphic marker in two Indian Ocean cores. Combined, these measurements make it possible to discuss the synchronism of the signals worldwide, within limits provided by astronomical tuning strategies, and to constrain the transition age for sediments deposited in different environments.

2. Sampling sites

Two equatorial cores MD90-949 (2°06.90′N, 76°06.50′E) and MD90-961 (5°03.71′N, 73°52.57′E) were collected in the Indian Ocean (Fig. 1) during the Seymama cruise of the French R/V Marion Dufresne east of the Maldives platform (Indian Ocean) at 3600 m and 2446 m water depth, respectively. Sediment from both cores has similar biogenic carbonate concentrations of 67 ± 5.5% and 64 ± 6%, respectively, within the intervals that contain the last reversal. Note, however, that the mean sediment accumulation rate at the deeper site MD90 949 was half that at site MD90-961 over the past 800 kyr. In addition, we present $\delta^{18}O$, magnetic, and microtektite records from a third southern equatorial sediment core (MD90-940, 5.35°S; 61.40°E) from the Indian Ocean (Meynadier et al., 1994) that was taken at a 3189 m water depth and is characterized by high biogenic carbonate contents with a mean value of 81 ± 6.5%.

Core MD95-2016 is a 33 m core that was taken at 2318 m water depth (57.4°N, 29.2°W) on Reykjanes Ridge (Fig. 1), North Atlantic Ocean, during the IMAGE 1 cruise of R/V Marion Dufresne. This high-latitude core can be compared with the other low-latitude records. It is composed of calcareous nanofossil-ooze with an average 21% biogenic carbonate content.

Core MD98-2183 (2°00.82′N, 135°01.26′E) was taken by the R/V Marion Dufresne during the IMAGE IV cruise at 4600 m water depth (Fig. 1), close to the carbonate compensation depth. The sediment consists of hemipelagic clay with calcareous nanofossils and more abundant siliceous microfossils. This core was formerly studied by Yamazaki and Oda (2004, 2005) to confirm the existence of 100-kyr inclination cycles that were initially reported in the nearby core MD98-2185.

All cores were sampled using 8 cm^3 cubes for stable isotopic analyses, ^{10}Be measurements, and magnetic parameters. In addition, U-channels were taken almost systematically. In all cases, it has been possible to obtain a continuous composite record. In some cases, the large core diameters made it possible to duplicate measurements at the same stratigraphic levels. This sampling protocol restrained uncertainties concerning the respective positions of the duplicate samples to a few millimeters at most.

3. Experiments

3.1. Magnetics

The measurements can be divided in three categories. Magnetic analyses were performed on U-channels and/or on adjacent single samples. Alternating field (AF) demagnetization of the natural remanent magnetization (NRM) was carried out with at least 8 steps on single samples from 2 cm stratigraphic intervals in all cores within and outside the transition intervals as well as on U-channel samples using a 2G-Enterprises cryogenic magnetometer. Rock magnetic parameters were measured at the same stratigraphic levels as the NRM. They included acquisition and stepwise AF demagnetization of anhysteretic remanent magnetization (ARM), down-core changes in low-field magnetic susceptibility, and S-ratio determination. These magnetic parameters undergo no major changes over the transition interval (Valet et al., 2016) which supports the standard quality criteria for RPI determination (King et al., 1983; Tauxe, 1993). Relative paleointensity (RPI) was estimated from the slope of the best fitting line passing through the NRM versus ARM data measured at the same successive demagnetization levels. Final RPI determinations were calculated from at least 6 successive demagnetization levels.

3.2. Beryllium

The ^{10}Be concentrations measured in marine sediments do not only depend on atmospheric ^{10}Be production rates but also on environmental conditions that affect the chemical and granulometric composition of sediments (Bourlès et al., 1989; Robinson et al., 1995). Absolute ^{10}Be concentrations of marine sediments are inversely proportional to carbonate content (Henken-Mellies et al., 1990) and proportional to the surface of the settling particles (Simon et al., 2016a). Thus, total ^{10}Be concentration must be corrected for environmental effects by normalizing the ^{10}Be concentration to the concentration of the stable ^{9}Be isotope associated with continental erosion. The ^{10}Be/^{9}Be ratio is subsequently refered as Be-ratio.

Samples of ∼1 g of dry sediment were processed for Be isotope analyses following the chemical procedure described by Bourlès et al. (1989) and revisited by Simon et al. (2016a). Both cosmogenic ^{10}Be and stable ^{9}Be isotopes have different sources, but their soluble form is homogenized in the water column before being scavenged and deposited by sinking particles. This requires a leaching procedure that extracts the authigenic phase of both isotopes – i.e. the fraction due to adsorption or chemical precipitation onto particles from sediments. The Be-ratio measured in this authigenic phase is equal to that of the overlying seawater at the time of deposition. The reader is referred to Bourlès et al. (1989); Ménabréaz et al. (2011, 2012); Valet et al. (2014); Simon et al. (2016b, 2018a) for thorough descriptions of the experimental protocol used for these experiments and results. Natural authigenic ^{9}Be concentrations were measured using a graphite-furnace atomic absorption spectrophotometer (AAS) with double-beam correction while ^{10}Be concentration measurements were performed after chemical preparation at the French accelerator mass spectrometer (AMS) national facility ASTER (CEREGE). Authigenic ^{10}Be concentrations are decay-corrected using the ^{10}Be half-life of 1.387 ± 0.012 Myr (Chmeleff et al., 2010; Korschinek et al., 2010).

3.3. Oxygen isotopes

The stable oxygen isotopic composition (δ^{18}O) of benthic and planktonic foraminifer species was determined at high-resolution (2–4 cm sampling intervals) using isotope ratio mass spectrometry (IR-MS) to derive bottom and surface water oceanographic/climatic signals and to develop a global stratigraphic framework linked to the waxing/waning of high-latitude ice caps.

For all cores, we analyzed the benthic species *Cibicides wuellestorfi* picked from the >150 μm size-fraction. Planktonic foraminifer species were picked in the narrower 250–315 μm size-fraction to avoid any size-dependent vital effects. We measured the isotopic composition of *Globigerina bulloides* in the high-latitude core MD95-2016. In low-latitude Indian Ocean cores, we analyzed the tropical shallow-dwelling species *Globigerinoides ruber* (core MD90-961) and *Globigerinoides trilobus* (more resistant to dissolution than *G. ruber* and thus preferentially preserved in deep cores MD90-940 and MD90-949). In core MD98-2183, only a benthic isotopic record could be obtained. This latter site is situated close to the carbonate compensation depth where dissolution of foraminifer shells during interglacial periods has removed most of the more fragile planktonic foraminifer shells, and left mostly benthic shells that are more resistant to dissolution.

Prior to isotopic analyses, the foraminifer shells were cleaned from fine particles through ultrasonication in methanol and were let to dry overnight at room temperature after the excess alcohol had been removed. Depending on the amount of available carbonate, analyses were performed on VG-Optima or Elementar Isoprime dual-inlet mass spectrometers. All results are expressed as δ^{18}O vs V-PDB (in ‰). The external analytical reproducibility determined from replicate measurements of a laboratory carbonate standard is ±0.05‰ (1σ). The singular value obtained for the international calcite standard NBS-18 is −23.27‰.

4. Synchronism between ^{10}Be and paleointensity changes

^{10}Be is produced in the upper atmosphere from spallation of oxygen and nitrogen by incoming charged and highly energetic galactic cosmic ray particles. Production is controlled by the position of the cut-off rigidity which is the limit that cosmic rays must exceed to reach the top of the atmosphere. The cut-off rigidity depends upon latitude and upon the geomagnetic dipole moment. Modulation of ^{10}Be by the geomagnetic field intensity is negligible close to the poles because the same quantity of incident charged particles is always trapped by the field lines. It is, however, strong at low latitudes where the position of the cut-off rigidity changes with field intensity. Therefore, variable amounts of incident galactic and cosmic protons are captured at low latitudes. Altogether, atmospheric mixing averages latitudinal ^{10}Be variations over the 1–2 yr residence time of this element in the atmosphere (Heikkilä et al., 2009), so that the dipole field strength is the primary factor that controls global variations of atmospheric cosmogenic production rates. Thus, the same amount of ^{10}Be overproduction is expected worldwide at the same time during field reversals that are characterized by dipole moment collapse. This observation holds by definition for a dipolar field, but is also valid for multipolar fields since spatial ^{10}Be production variability should be homogenized by atmospheric circulation.

Differences in ^{10}Be distributions among sediment cores can result from how ^{10}Be is incorporated within sediments. Larger amplitude production peaks are expected in sediments with lower deposition rates, and conversely a wider distribution of values and smaller peak amplitude are expected for rapid accumulation rates. However, the same total amount of ^{10}Be is incorporated during the same time interval and, therefore, the maximum production peak should occur at the same time at all sites. Stratigraphic offsets between peaks of ^{10}Be maximum production are unlikely to be generated by changes in adsorption processes onto sediment particles or by mixing within the sediment. Bioturbation smears the ^{10}Be record, but it does not move the signal further down within the sediment column (Suganuma et al., 2010; Valet et al., 2014). Consequently, the stratigraphic position of the maximum ^{10}Be production peak within a sediment should coincide with the period of lowest geomagnetic intensity, which is evident as a worldwide temporal marker of the last polarity reversal.

As discussed above, geomagnetic reversals may not be globally synchronous. As long as the field is dipolar there is worldwide synchronism of dipole field intensity changes with short time scales during a reversal and magnetic records must coincide during this period. Therefore, offsets or delays can only result from magnetization processes within the sediment, particularly post-depositional reorientation of magnetic particles (Verosub, 1977; DeMenocal et al., 1990; Roberts and Winklhofer, 2004). For this reason, it is crucial to combine ^{10}Be and magnetic data from the same samples to determine potential offsets between the two signals and understand their significances (Valet et al., 2014).

5. Results and discussion

5.1. Be-ratio and directional changes

In Fig. 2a, b, e, f we show the evolution of the Be-ratio measured in the four cores as a function of depth. In each case, the initial Be-ratio records are plotted along with the results of a slight smoothing by weighted average that involves 5% of the datapoints. This approach avoids uncertainties generated by high-frequency changes and constrains further the position of the Be-peaks. The

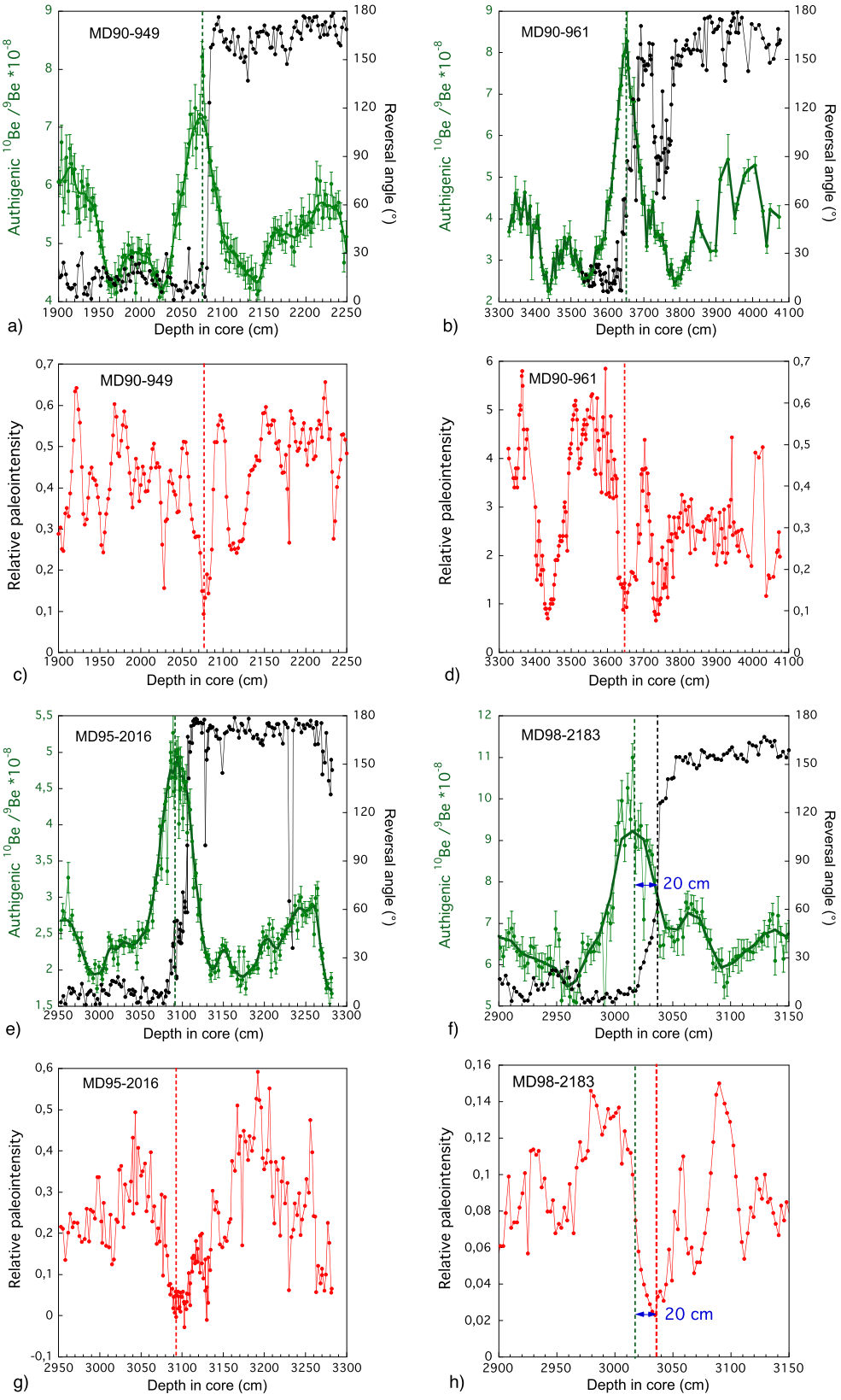

Fig. 2. (a, b, e, f) Be-ratio with associated error bars (green lines) and reversal angle (black lines) as a function of depth across the last reversal in the four studied cores. Thick green curves correspond to slight smoothing of the Be-ratio by weighted average. Vertical dashed lines indicate the position of maximum beryllium production during the last reversal. (c, d, g, h) Relative paleointensity across the same depth interval as for the Be-ratio. Vertical red dashed lines show the position of the mid-transitional direction. Note the 20 cm offset between the Be-ratio peak and the magnetic mid-reversal position in core MD98-2183.

vertical green dashed line indicates the position of each Be-ratio peak. In the same plots are also shown the evolution of the reversal angle measured from the direction of the axial dipole at each site (Valet et al., 2016). This representation depicts the actual field evolution at each site and does not require assumptions required for calculation of virtual geomagnetic poles. Given the large scatter and overall low quality of demagnetization diagrams associated with transitional periods (discussed in Valet et al., 2016) we have little confidence in detailed interpretation of transitional directions. However, all reverse and normal polarity directions are clearly defined and constrain the boundaries of the transition. The record from core MD90-949 has a regular Be-ratio peak and a sharp directional transition. This is expected given the low sediment accumulation rate ($v = 2.0$ cm/ka). The nearby core MD90-961 has a twofold larger deposition rate (4.2 cm/ka) with similar characteristics for the Be-ratio peak, and a longer magnetic transition. It is significant that in both cores there is no offset between the Be-ratio peak and the transition. The same situation prevails for core MD95-2016 (north Atlantic Ocean), which is characterized by a similar Be-ratio peak and a regular evolution of transitional directions. Not surprisingly, this record has similarities with results from core MD90-961 because both have equivalent resolution (3.1 cm/ka).

RPI variations within each core have also been plotted in Fig. 2c, d, g, h on the same depth scale. In all cases (except for core MD98-2183) the RPI minimum coincides with the transitional interval as well as with the Be-ratio maximum. Outside the reversal we note, however, that the Be-ratio and RPI signals do not always match each other. This complex situation depends on several factors that go beyond the scope of this paper and that will be presented and discussed elsewhere. The fact that in all cases the Be-ratio and RPI records have the largest amplitude changes in concordance with each other during the reversal is a strong indication of their geomagnetic origin.

Core MD98-2183 is the unique case in which there is a significant offset of about 20 cm between the Be-ratio peak and both directional and RPI variations that characterize the polarity transition (Fig. 2). Similar offsets have also been observed elsewhere in cores from the Portuguese margin (Carcaillet et al., 2003, 2004), western Philippine Sea (Simon et al., 2018b) and western equatorial Pacific Ocean (Suganuma et al., 2010). In contrast to the other reversal records, demagnetization diagrams for transitional samples are of good quality (Valet et al., 2016). Successive transitional directions undergo a progressive declination rotation while inclination remains close to 0° in accordance with the site latitude. This behavior results from smearing of magnetic directions induced by progressive post-depositional orientation of magnetic grains imposed by stronger fields in the subsequent stable normal polarity state.

Summarizing, sediments from the two equatorial Indian Ocean cores and from the north Atlantic Ocean core do not provide any indication of delayed magnetization, but rather they record synchronous ^{10}Be production, RPI and directional changes at each site. Only the sediment from the Equatorial Western Pacific Ocean has a magnetization acquisition that is offset by about 20 cm, that is about 5 kyr delay, with respect to the maximum ^{10}Be production.

5.2. Microtektite layers

Another stratigraphic marker is the microtektite layer associated with the Australasian microtektite event which is well documented in Indochina, southern China, the Philippines, Malaysia, Indonesia, and Australia. The source crater remains unknown, but the microtektites were produced about 12–15 kyr prior to the last reversal (Glass et al., 1979; Schneider and Kent, 1990; Suganuma et al., 2011). Microtektite analysis has been carried out for core MD90-961 and the results have been presented and discussed in comparison with previous studies from the Sulu and Celebes seas (Valet et al., 2014; Suganuma et al., 2011). The amplitude of the depth offset between the last reversal and the Be-ratio peak is correlated with deposition rate. This situation is unlikely in presence of late magnetization acquisition because it would change the depths independently of the accumulation rate. Here, we add new results (Fig. 3a, c) from core MD90-949 and from the 32 m-long core MD90-940 (61°40.12E, 05°33.53S) from Madingley Rise (Fig. 3b). We did not find microtektites in core MD98-2183 despite their presence in nearby core MD98-2187 (Yamazaki and Oda, 2005; Suganuma et al., 2011). The number of counted microtektites in the three layers are compared in Fig. 3a and plotted as percentage of their maximum number in each core in Fig. 3b, c, d. In all cases, bioturbation has generated an asymmetrical tektite distribution over a 20 cm sediment thickness with a sharp increase and a progressive upward decrease.

In Fig. 3b, c, d are shown the oxygen isotope records, the positions of the Be-ratio peak, and angular deviation as a function of depth in each core. In the three Indian Ocean cores the maximum occurrence of microtektites (vertical red dashed lines) occurs at the same stratigraphic position at the beginning of the marine isotope stage (MIS) 20/19 transition. The mid-reversal position derived from the Be-ratio peak position (vertical green dashed line) in cores MD90-949 (Fig. 3c) and MD90-961 (Fig. 3d) coincides with the location of the directional changes as well as with the RPI minima (Fig. 2c, d). We, therefore, infer that there is no stratigraphic ambiguity for the reversal position during MIS 19 from these marine sedimentary sequences.

5.3. ^{10}Be and marine isotope stages

The observed synchronism between cosmogenic and magnetic changes clearly indicates the coherence of these records that allows to define an accurate mid-reversal position from two independent proxies. We can now compare the position of each Be-ratio peak with the δ^{18}O record obtained at the same site. The results are plotted as a function of depth for each of the four studied cores (Fig. 4a, b, c, d). The results indicate that maximum ^{10}Be production was incorporated in all sediments immediately after the warmest period of MIS 19, i.e. just after the MIS 19c interglacial. This period cannot be identified in the δ^{18}O record of MD98-2183 due to poor foraminifera abundance during this period. However, the MIS 20 signature is preserved and is found prior to the Be-ratio peak, consistent with the other three records. We, thus, infer that the mid-reversal position occurred after the MIS 19 maximum at all four sites within the limits of correlation.

An age model was constructed by assigning a common depth derived from correlation of individual δ^{18}O curves to the composite record of sister cores MD90-961/963 (Bassinot et al., 1994; Valet et al., 2014). The MD90-961/963 record was chosen as our internal reference record because of its higher sedimentation rate and its higher resolution isotopic record. Once all of the individual cores had been depth-correlated to core MD90-961/963, the age model was developed by tuning the benthic δ^{18}O record from core MD90-961/963 to the LR04 global benthic stack of Lisiecki and Raymo (2005). Using this strategy, we have a set of cores for which the ages of the Be-ratio peaks and RPI minima can be determined from a coherent stratigraphic framework.

By applying such dating strategy, we assume that oxygen isotope changes are synchronous worldwide. Over the last decade, however, several works have proven such assumption to be invalid, revealing potential offsets of a few thousand years between δ^{18}O records from different oceanic basins or from different water masses within the same basin (Skinner and Shackleton, 2005; Lisiecki and Raymo, 2009; Waelbroeck et al., 2011; Stern and

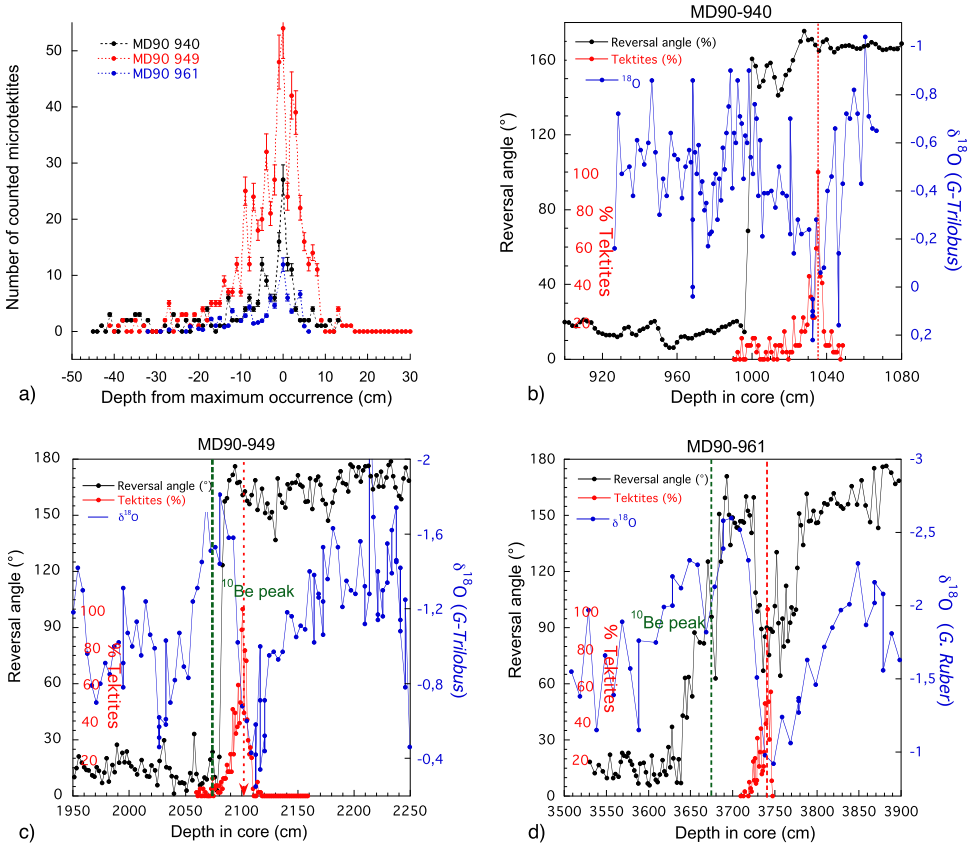

Fig. 3. (a) Number of counted microtektites as a function of depth in cores MD90-940, MD90-949 and MD90-961 from the equatorial Indian Ocean. (b–c–d) Changes in $\delta^{18}O$ (blue lines), reversal angle (dark lines) and percentage of microtektites (red lines) in the same cores. Vertical green dashed lines show the position of maximum Be-ratio. Vertical red dashed lines correspond to maximum counted microtektites number.

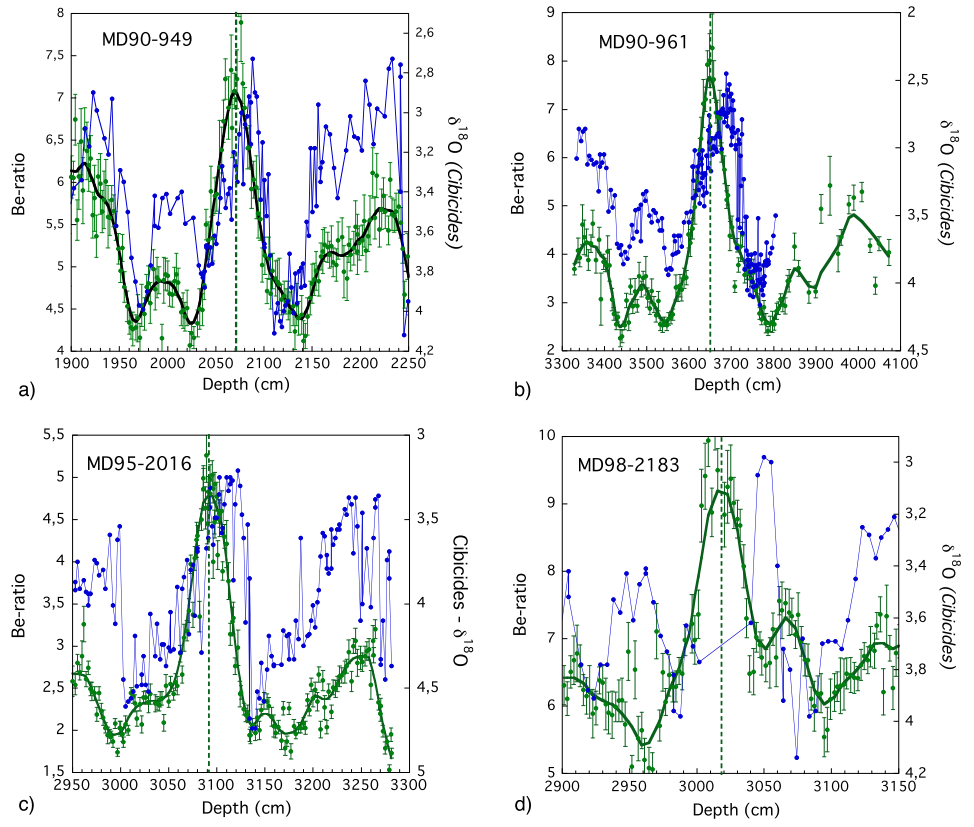

Fig. 4. Be-ratio (green lines) and $\delta^{18}O$ curves (blue lines) as a function of depth in cores MD90-949 (a), MD90-961 (b), MD95-2016 (c) and MD98-2183 (d). Vertical green dashed lines give the position of maximum Be-ratio.

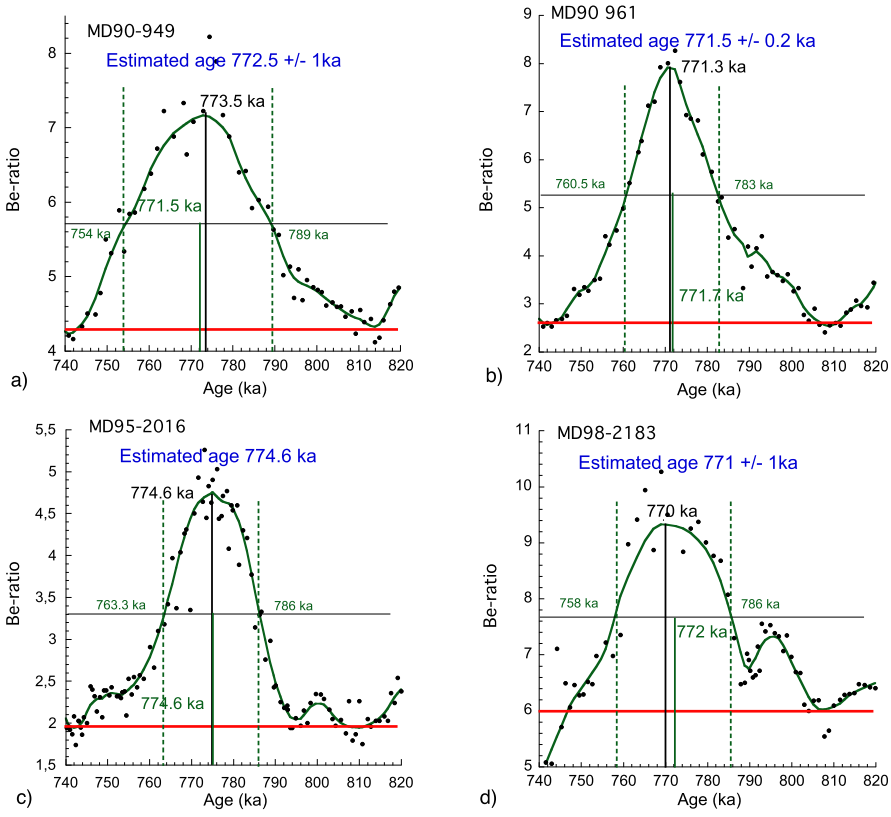

Fig. 5. Be-ratio as a function of age in cores MD90-949 (a), MD90-961 (b), MD95-2016 (c) and MD98-2183 (d). Original Be-ratio values (black dots) have been slightly smoothed by weighted average (green lines). Vertical black lines give the age of the corresponding maximum Be-ratios. Red lines indicate the Be-ratio baseline in each core. Horizontal black lines show the Be-ratio mid-peak values while dashed vertical green lines indicate their lower and upper ages. Green vertical lines give the age of the interval mid-peak assuming a similar Gaussian shape for all Be-ratio records. The difference between the two techniques (maximum Be-ratio and mid-peak) is our best approximation of error on the age of maximum atmospheric ^{10}Be production.

Lisiecki, 2014). Those works have been fueled by the seminal study of Skinner and Shackleton (2005), which showed – based on high-resolution planktonic ^{14}C age models – that the middle of the last termination deep Pacific benthic δ^{18}O lagged the deep North Atlantic by 3.9 kr due to a delayed temperature response. It has been concluded, however, that such regional time offsets are only important during glacial terminations due to major reorganization of ocean circulation and complex interplay of temperature changes and deglacial δ^{18}O transit time in the ocean water masses (e.g., Lisieki and Stern, 2016). The B/M reversal did not occur during the deglaciation from MIS20 to MIS19, but well into the MIS19, after the full interglacial MIS19c. It is our contention that regional offsets between δ^{18}O records were likely minimal during late MIS19 and the progressive transition to MIS18. Thus, potential age errors introduced by assuming the synchronism of benthic δ^{18}O records are much less important than uncertainties associated with the graphical alignment of δ^{18}O curves obtained from our low-sedimentation rate deep-sea cores.

Be-ratio changes measured between 740 ka and 810 ka are plotted in Fig. 5. As in the previous figures, the Be-ratio records have been smoothed slightly (green lines) to eliminate high-frequency changes. Also shown in each case is a reference baseline (red horizontal line) that is useful for comparing the relative amplitude of ^{10}Be production between each site. This baseline was also helpful to define the center of the mid-peak level and, thus, to check the consistency between two different age determinations derived from the position of the Be-ratio peak (black lines in Fig. 5) and the position of the mid-height of the peak (green lines in Fig. 5), respectively. We assumed that the shape of the Be-ratios can be roughly approximated by a Gaussian distribution, which allow us to estimate an error on the ages of the peaks.

In all cases, the ages of the Be-ratio peaks are very close or coincide with those derived from the mid-peak. The Indian and Pacific Ocean results are consistently found at 772.5 ± 1 ka and 771.5 ± 0.2 ka for the two Indian Ocean cores, 771 ± 1 ka for the western Pacific, while the Atlantic dataset is characterized by a slightly older age at 774.6 ka. These results yield a mean age of 772.4 ± 1.6 ka for all records. When taking into account additional uncertainties associated with the age model of LR04 and our alignment to this target curve (i.e. ∼ ±5 ka), our mean age estimate for the B-M transition is 772.4 ± 6.6 ka.

Is the difference with the Atlantic record significant? Coincidence or not, an age of 773.1 ka was obtained from five nearby north Atlantic Ocean cores with rapid accumulation rates (Channell et al., 2010). In Fig. 6a the upper part of all Be-ratio peaks has been plotted as a function of age after rescaling with respect to the maximum peak values. The vertical bars indicate the lower (771.8 ka) and upper (774 ka) age limits that were defined above for the Be-ratio peak. We followed the same approach in Fig. 6b for the RPI minima normalized with respect to their mean value over the same time interval. As expected and discussed above, late magnetization acquisition process inherent to core MD98-2183 generated a 15 kyr delay of the RPI minimum with respect to the Be-ratio peak. In Fig. 6c the magnetic data of this core have been re-plotted after correcting for the 20 cm offset between the two signals. The results show that the paleointensity minima of all cores lie within the age limits of 772.4 ± 1.6 ka defined above and furthermore within the time interval 765.8–779 ka when considering the uncertainty of 6.6 ka associated with the age model of LR04.

We infer that the relative uncertainty on the mid-reversal age does not exceed ±6.6 ka. Causes of error are linked to the mor-

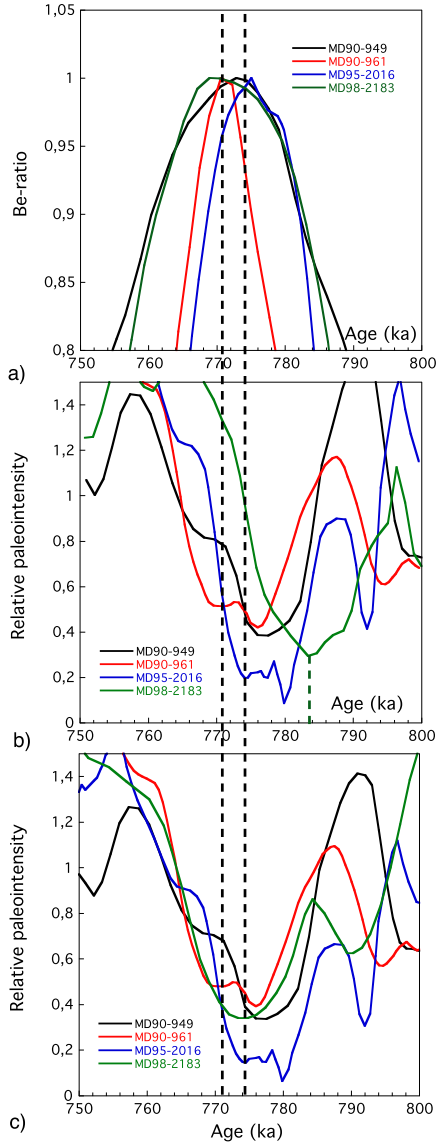

Fig. 6. Enlarged view of (a) the upper part of the authigenic $^{10}Be/^{9}Be$ ratio (normalized) changes and (b) lower part of the paleointensity minimum during the reversal as a function of age with the age offset of the RPI signal in core MD98-2183. (c) same as (b) after correcting the RPI signal of MD98-2183 for 20 cm stratigraphic delay with respect to the Be-ratio peak.

phology of the Be-ratio records and to the quality of the depth-age correlation constrained by the oxygen isotope records. Therefore, the differences among the Atlantic and other records cannot be considered as significant in the present state of the art and, most importantly, we cannot reconcile the potential errors with ca 10 kyr older age as recently inferred from chronologies using interpolation between radiometric dating (Sagnotti et al., 2016; Mark et al., 2017).

6. Conclusion

In this study, we present detailed and independent analyses of Be-ratio, paleomagnetic directions, relative paleointensity, and oxygen isotopes from four marine sediment cores covering the last geomagnetic reversal, i.e., the Matuyama–Brunhes transition. This is likely the most complete dataset obtained so far for this time period. Those measurements were complemented by microtektite analyses for three Indian Ocean cores prior to the reversal. At three sites, we observe synchronism between the magnetic and cosmogenic records, which demonstrates the potential of this dataset to define the most accurate reversal position from independent proxies. The equatorial western Pacific Ocean is the only record studied here that revealed an offset between the RPI minima and the Be-ratio peak, which is caused by a delayed magnetization lock-in of 20 cm which represents about 5 kyr. The age of the Matuyama–Brunhes reversal was derived from Be-ratio peaks and is fully consistent with the intensity minima and directional changes. The depth-time model derived from the correlation of the $\delta^{18}O$ records with the Lisiecki and Raymo (2005) LR04 global benthic stack indicates that the field reversed polarity at 772.4 ± 1.6 ka within our common chronostratigraphic frame, and 772.4 ± 6.6 ka when taking into account a potential age uncertainty of ±5 ka associated with the tuning strategy used for deriving the age model of LR04 and our alignment to this target curve. This age estimate is consistent with all recent dates that have been obtained from orbitally tuned paleomagnetic records. They differ from the ca 10 ka older age recently derived from radiometric dating of tephra layers found in a marine sediment core (Mark et al., 2017). However, we cannot exclude that the reversal position was not accurately defined in the ODP 758 sediment used for that study (Channell and Hodell, 2017), as this reversal clearly occurs before the optimum of MIS19 in ODP-758, whereas we observe it consistently after MIS19c in all our records. There can be variable definitions of reversal boundaries that contribute to the repartition of different ages for this reversal. For levels that mark the onset of the Be-ratio peak we obtain an age of 786 ± 2 ka (786 ± 7 ka when taking into account uncertainties associated to LR04 and the alignment to this target curve) that is consistent with the older radiometric age. Determining the middle of the transition can be difficult when referring to poorly defined transitional directions, except for rapidly deposited records (Valet et al., 2016; Channell, 2017). Therefore, it is justified to determine the age of the reversal using the period of lowest field intensity, which should coincide with the period of maximum ^{10}Be production. This condition was met in the present study, which enables the definition of reversal position.

Acknowledgements

The authors thank F. Dewilde (LSCE) for oxygen isotope analyses and G. Isguder for foraminifer controls, Anojh Thevarasan (IPGP) for magnetic measurements and Laetitia Gacem and Sandrine Choy (CEREGE) for chemical preparation before Be analyses. This research was funded by the European Research Council (ERC) under the European Union's Seventh Framework Programme (FP7/2007–2013)/ERC advanced grant agreement GA 339899. This is IPGP contribution #3991 and LSCE contribution #6521.

References

Balbas, A., Koppers, A.P., Clark, P.U., Coe, R.S., Reilly, B., Stoner, J., Konrad, K., 2018. Millennial scale instability in the geomagnetic field prior to the Matuyama–Brunhes reversal. Geochem. Geophys. Geosyst. https://doi.org/10.1002/2017GC007404.

Bassinot, F.C., Labeyrie, L.D., Vincent, E., Quidelleur, X., Shackleton, N.J., Lancelot, Y., 1994. Earth Planet. Sci. Lett. 126 (1–3), 91–108.

Bourlès, D., Raisbeck, G.M., Yiou, G.M., 1989. ^{10}Be and ^{9}Be in marine sediments and their potential for dating. Geochim. Cosmochim. Acta 53, 443–452. https://doi.org/10.1016/0016-7037(89)90395-5.

Carcaillet, J.T., Bourlès, D.L., Thouveny, N., 2004. Geomagnetic dipole moment and ^{10}Be production rate intercalibration from authigenic $^{10}Be/^{9}Be$ for the last 1.3 Ma. Geochem. Geophys. Geosyst. 5 (5), Q05006. https://doi.org/10.1029/2003GC000641.

Carcaillet, J.T., Thouveny, N., Bourlès, D.L., 2003. Geomagnetic moment instability between 0.6 and 1.3 Ma from cosmonuclide evidence. Geophys. Res. Lett. 30 (15), 1792. https://doi.org/10.1029/2003GL017550.

Channell, J.E.T., Hodell, D.A., Singer, B.S., Xuan, C., 2010. Reconciling astrochronological and $^{40}Ar/^{39}Ar$ ages for the Matuyama–Brunhes boundary and late Matuyama chron. Geochem. Geophys. Geosyst. 11. https://doi.org/10.1029/2010GC003203.

Channell, J.E.T., 2017. Complexity in Matuyama–Brunhes transitions from North Atlantic IODP/ODP deep-sea sites. Earth Planet. Sci. Lett. 467, 43–56.

Chmeleff, J., von Blankenburg, F, Kossert, K., Jakob, D., 2010. Determination of the ^{10}Be half-life by multicollector ICP-MS and liquid scintillation counting. Nucl. Instrum. Methods Phys. Res. 268 (2), 192–199.

Courtillot, V., Gallet, Y., LeMouël, J.L., Fluteau, F., 2007. Are there connections between the Earth's magnetic field and climate? Earth Planet. Sci. Lett. 253, 328–339.

DeMenocal, P., Ruddiman, W.F., Kent, D.V., 1990. Depth of post-depositional remanence acquisition in deep-sea sediments: a case study of the Brunhes–Matuyama reversal and oxygen isotopic stage 19.1. Earth Planet. Sci. Lett. 99 (1–2), 1–13.

Evans, M.E., Muxworthy, A.R., 2018. A re-appraisal of the proposed rapid Matuyama–Brunhes geomagnetic reversal in the Sulmona basin, Italy. Geophys. J. Int. 213, 1744–1750.

Glass, B.P., Swincki, M.B., Zwart, P.A., 1979. Australasian, ivory coast and North American tektite strewn fields: size, mass and correlation with geomagnetic reversals and other Earth events. In: Proc. Lunar Planet. Sci. Conf., vol. 10, pp. 2535–2545.

Heikkilä, U., Beer, J., Feichter, J., 2009. Meridional transport and deposition of atmospheric ^{10}Be. Atmos. Chem. Phys. 9, 515–527.

Henken-Mellies, W.U., Beer, J., Heller, F., Hsu, K.J., Shen, C., Bonani, G., Hofmann, H.J., Super, M., Wölfli, W., 1990. ^{10}Be and ^{9}Be in South Atlantic DSDP Site 519: relation to geomagnetic reversals and to sediment composition. Earth Planet. Sci. Lett. 98, 267–276.

King, J.W., Banerjee, S.K., Marvin, J., 1983. A new rock-magnetic approach to selecting sediments for geomagnetic paleointensity studies: application to paleointensity for the last 4000 years. J. Geophys. Res. 88, 5911–5921.

Kong, X., Zhou, W., Beck, J.W., Xian, F., Zherkun, W., 2014. Asynchronous records of Brunhes–Matuyama reversal in marine sediments and Chinese loess: review and discussion. Quat. Int. 319, 137–142.

Korschinek, G., Bergmaier, A., Faestermann, T., Gerstmann, U.C., Knie, K., Rugel, G., Wallner, A., Dillmann, I., Dollinger, G., Lierse von Gostomski, Ch., Kossert, K., Maiti, M., Poutivtsev, M., Remmert, A., 2010. A new value for the half-life of ^{10}Be by heavy-ion elastic recoil detection and liquid scintillation counting. Nucl. Instrum. Methods Phys. Res., Sect. B, Beam Interact. Mater. Atoms 268 (2), 187–191. https://doi.org/10.1016/j.nimb.2009.09.020.

Leonhardt, R., Fabian, K., 2007. Paleomagnetic reconstruction of the global geomagnetic field evolution during the Matuyama–Brunhes transition: iterative Bayesian inversion and independent verification. Earth Planet. Sci. Lett. 253, 172–195.

Lisiecki, L.E., Raymo, M., 2009. Diachronous benthic δ^{18}O responses during late Pleistocene terminations. Paleoceanography 24. https://doi.org/10.1029/2009P1001732.

Lisiecki, L.E., Stern, J.V., 2016. Regional and global benthic δ^{18}O stacks for the last glacial cycle. Paleoceanography 31. https://doi.org/10.1002/2016PA003002.

Lisiecki, L.E., Raymo, M.E., 2005. A Pliocene–Pleistocene stack of 57 globally distributed benthic delta ^{18}O records. Paleoceanography 20, PA1003. https://doi.org/10.1029/2004PA001071.

Mark, D.F., Renne, P.R., Dymock, R.C., Smith, V.C., Simon, J.I., Morgan, L.E., Staff, R.A., Ellis, B.S., Pearce, N.J.G., 2017. High-precision ^{40}Ar/^{39}Ar dating of pleistocene tuffs and temporal anchoring of the Matuayam–Brunhes boundary. Quartern. Geochron. 39, 1–23.

Ménéabraz, L., Bourlès, D.L., Thouveny, N., 2012. Amplitude and timing of the Laschamp geomagnetic dipole low from the global atmospheric ^{10}Be overproduction: contribution of authigenic ^{10}Be/^{9}Be ratios. J. Geophys. Res. 117 (B11). https://doi.org/10.1029/2012jb009256.

Ménéabraz, L., Thouveny, N., Bourlès, D.L., Deschamps, P., Hamelin, B., Demory, F., 2011. The Laschamp geomagnetic dipole low expressed as a cosmogenic ^{10}Be atmospheric overproduction at 41 ka. Earth Planet. Sci. Lett. 312, 305–317.

Meynadier, L., Valet, J.-P., Bassinot, F., Shackleton, N., Guyodo, Y., 1994. Asymmetrical saw-tooth pattern of the geomagnetic field intensity from equatorial sediments in the Pacific and the Indian oceans. Earth Planet. Sci. Lett. 126, 109–127.

Olson, P.L., Glatzmaier, G.A., Coe, R.S., 2011. Complex polarity reversals in a geodynamo model. Earth Planet. Sci. Lett. 304, 168–179.

Robinson, C., Raisbeck, G.M., Yiou, F., Lehman, B., Laj, C., 1995. The relationship between ^{10}Be and geomagnetic field records in central North Atlantic sediments during the last 80 ka. Earth Planet. Sci. Lett. 136 (3–4), 551–557.

Sagnotti, L., Giaccio, B., Liddicoat, J.C., Sprain, C., 2016. How fast was the Matuyama–Brunhes geomagnetic reversal? A new subcentennial record from the Sulmona Basin, central Italy. Geophys. J. Int. 204 (2), 798–812. https://doi.org/10.1093/gji/ggv486.

Schneider, D.A., Kent, D.V., 1990. Ivory coast microtektites and geomagnetic reversals. Geophys. Res. Lett. 17, 163–166.

Simon, Q., Thouveny, N., Bourlès, D.L., Bassinot, F., Savranskaia, T., Valet, J.P., ASTER Team, 2018a. Increased production of cosmogenic ^{10}Be recorded in oceanic sediment sequences: information on the age, duration, and amplitude of the geomagnetic dipole moment minimum over the Matuyama–Brunhes transition. Earth Planet. Sci. Lett. 489, 191–202.

Simon, Q., Bourlès, D.L., Thouveny, N., Horng, C.-H., Valet, J.P., Bassinot, F., Choy, S., 2018b. Cosmogenic signature of geomagnetic reversals and excursions from the Reunion event to the Matuyama–Brunhes transition (0.7–2.14 Ma interval). Earth Planet. Sci. Lett. 482, 510–524.

Simon, Q.S., Thouveny, N., Bourlès, D., Nuttin, L., Hillaire-Marcel, C., St-Onge, G., 2016a. Authigenic ^{10}Be/^{9}Be ratios and ^{10}Be fluxes (^{230}Thxs normalized) in central Baffin Bay sediments during the last glacial cycle: paleoenvironmental implications. Quat. Sci. Rev. 104, 142–162.

Simon, Q., Thouveny, N., Bourlès, D.L., Valet, J.P., Bassinot, F., Ménabréaz, L., Guillou, V., Choy, S., Beaufort, L., 2016b. Authigenic ^{10}Be/^{9}Be ratio signatures of the cosmogenic nuclide production linked to geomagnetic dipole moment variation since the Brunhes/Matuyama boundary. J. Geophys. Res. 121. https://doi.org/10.1002/2016JB013335.

Singer, B.S., Pringle, M.S., 1996. Age and duration of the Matuyama–Brunhes geomagnetic polarity reversal from ^{40}Ar/^{39}Ar incremental heating analyses of lavas. Earth Planet. Sci. Lett. 139, 47–61.

Singer, B.S., Relle, M.R., Hoffman, K.A., Battle, A., Guillou, H., Laj, C., Carracedo, J.C., 2002. ^{40}Ar/^{39}Ar ages from transitionally magnetized lavas on La Palma, Canary islands, and the geomagnetic instability timescale. J. Geophys. Res. 107 (B11), 2307. https://doi.org/10.1029/2001JB001613.

Skinner, L., Shackleton, N.J., 2005. An Atlantic lead over Pacific deep-water change across termination I: implications for the application of the marine isotope stage stratigraphy. Quat. Sci. Rev. 24 (5–6), 571–580. https://doi.org/10.1016/j.Quat.Sci.Rev.2004.11.008.

Stern, J.V., Lisiecki, L.E., 2014. Termination 1 timing in radiocarbon-dated regional benthic δ^{18}O stacks. Paleoceanography 29, 1127–1142. https://doi.org/10.1002/2014PA002700.

Suganuma, Y., Yokoyama, Y., Yamazaki, T., Kawamura, K., Horng, C.S., Matsuzaki, H., 2010. ^{10}Be evidence for delayed acquisition of remanent magnetization in marine sediments: implication for a new age for the Matuyama–Brunhes boundary. Earth Planet. Sci. Lett. 296, 443–450.

Suganuma, Y., Okuno, J., Heslop, D., Roberts, A., Yamazaki, T., Yokoyama, Y., 2011. Post-depositional remanent magnetization lock-in for marine sediments deduced from ^{10}Be and paleomagnetic records through the Matuyama–Brunhes boundary. Earth Planet. Sci. Lett. 311 (1–2), 39–52.

Tauxe, L., 1993. Sedimentary records of relative paleointensity of the geomagnetic field: theory and practice. Rev. Geophys. 31, 319–354.

Thouveny, N., Bourlès, D.L., Saracco, G., Carcaillet, J.T., Bassinot, F., 2008. Paleoclimatic context of geomagnetic dipole lows and excursions in the Brunhes, clue for an orbital influence on the geodynamo? Earth Planet. Sci. Lett. 275 (3–4), 269–284. https://doi.org/10.1016/j.epsl.2008.08.020.

Valet, J.P., Fournier, A., 2016. Deciphering records of geomagnetic reversals. Rev. Geophys. https://doi.org/10.1002/2015RG000506.

Valet, J.P., Plenier, G., 2008. Simulations of a time-varying non dipole field during geomagnetic reversals and excursions. Phys. Earth Planet. Inter. 169 (1–4), 178–193. https://doi.org/10.1016/j.pepi.2008.07.031.

Valet, J.P., Bassinot, F., Bouilloux, A., Bourlès, D., Nomade, S., Guilloux, V., Lopes, F., 2014. Thouveny N., Geomagnetic, cosmogenic and climatic changes across the last geomagnetic reversal from Equatorial Indian Ocean sediments. Earth Planet. Sci. Lett. 397, 67–79.

Valet, J.P., Fournier, A., Courtillot, V., Herrero-Bervera, E., 2012. Dynamical similarity of geomagnetic field reversals. Nature 490, 89–94. https://doi.org/10.1038/nature1149.

Valet, J.P., Meynadier, L., Simon, Q., Thouveny, N., 2016. When and why sediments fail to record the geomagnetic field during polarity intervals. Earth Planet. Sci. Lett. 453, 96–107.

Verosub, K.L., 1977. Depositional and post-depositional processes in the magnetization of sediments. Rev. Geophys. Space Phys. 15, 129–143.

Waelbroeck, C., Skinner, L.C., Labeyrie, L., Duplessy, J.C., Michel, E., Vasquez Riveiros, N., Gherardi, J.M., Dewilde, F., 2011. The timing of deglacial circulation changes in the Atlantic. Paleoceanography 26, PA3213. https://doi.org/10.1029/2019PA002007.

Wang, R., Lovlie, R., 2010. Subaerial and subaqeous deposition of loess: experimental assessment of detrital remanent magnetization in Chinese loess. Earth Planet. Sci. Lett. 298 (3–4), 294–304.

Wang, X., Lovlie, R., Chen, Y., Yang, Z., Pei, J., Tang, L., 2014. The Matuyama–Brunhes polarity reversal in four Chinese loess records: high-fidelity recording of geomagnetic field behavior or a less than reliable chronostratigraphic marker? Quat. Sci. Rev. 101.

Worm, H.U., 1997. A link between geomagnetic reversals and events and glaciations. Earth Planet. Sci. Lett. 147, 55–67.

Yamazaki, T., Oda, H., 2004. Intensity-inclination correlation for long-term secular variation of the geomagnetic field and its relevance to persistent non-dipole components. In: Channell, J.E.T., Kent, D.V., Lowrie, W., Meert, J. (Eds.), Timescales of the Paleomagnetic Field, AGU Monograph, p. 328.

Yamazaki, T., Oda, H., 2005. A geomagnetic paleointensity stack between 0.8 and 3.0 Ma from equatorial Pacific sediment cores. Geochem. Geophys. Geosyst. 6, Q11H20. https://doi.org/10.1029/2005GC001001.

Zhao, X., Roberts, A.P., 2010. How does chinese loess become magnetized? Earth Planet. Sci. Lett. 292 (1–2), 112–122.

Zhou, W., Beck, J.W., Kong, X., An, Z., Qiang, X., Wu, Z., Xian, F., Ao, H., 2014. Timing of the Brunhes–Matuyama magnetic polarity reversal in Chinese loess using ^{10}Be. Geology 42 (6), 467–470. https://doi.org/10.1130/G35443.1.